Climate Dynamics
https://doi.org/10.1007/s00382-024-07143-z

ORIGINAL ARTICLE

Relating extreme precipitation events to atmospheric conditions and driving variables in China

Qianxi Ou[1] · Tongtiegang Zhao[1] · Shuo Wang[2] · Yang Liu[3] · Yongyan Wu[1] · Bo Li[1] · Xiaohong Chen[1]

Received: 30 August 2023 / Accepted: 3 February 2024

Abstract

Extreme precipitation events (EPEs) have garnered considerable social concerns due to their hazardous and destructive nature. To identify the possible causes of EPEs in China, this paper presents an in-depth investigation of how EPEs coincide with atmospheric conditions, i.e., atmospheric instability, moisture availability and moisture convergence, as well as driving variables, i.e., vertical velocity, relative humidity and air temperature. Specifically, the classic coincidence probability is devised to explicitly relate 72-h EPEs to convective available potential energy (CAPE), precipitable water (PW), vertical velocity at 700 hPa (verV), relative humidity at 700 hPa (RH), average air temperature between 850 and 500 hPa (Tavg) as well as air temperature difference between 850 and 500 hPa (Tdiff). The results show that at the annual timescale, EPEs in Southeast and Southwest China are dominantly controlled by verV, in North and Central China by PW and in Northwest China by CAPE roughly. At the seasonal timescale, the spatial distributions of coincidence probability values and "competition" among atmospheric conditions and driving variables exhibit similar patterns as observed throughout the entire year except for December–January–February. Moreover, the diagnostic plots generated for three case study regions in China provide valuable insights into the temporal evolution of precipitation events, cumulative distribution function curves of influential factors and dominant controlling factors of EPEs. This paper contributes to understandings of the dominant controlling factors of EPEs for the whole of China. The spatial patterns of EPEs and their related atmospheric conditions and driving variables yield useful information for rainstorm forecasting and disaster risk management.

Plain Language Summary

Atmospheric conditions, i.e., atmospheric instability, moisture availability and wind convergence, and driving variables, i.e., vertical velocity, relative humidity and air temperature, play important parts in the occurrence of extreme precipitation events (EPEs). In this paper, the 72-h EPEs in China are explicitly related to atmospheric conditions and driving variables by using the classic coincidence probability. Specifically, the relationships are measured by the ratio of the time when precipitation and the given factor both reaching at extreme to the whole time in EPEs. Assuming that the factor exhibiting the highest coincidence probability influences EPEs the most, it is observed that at the annual timescale, vertical velocity at 700 hPa has the greatest impact on EPEs in Southeast and Southwest China as well as part of Northeast China, precipitable water in North and Central China and convective available potential energy in Northwest China. Also, it is found that the

✉ Tongtiegang Zhao
zhaottg@mail.sysu.edu.cn

[1] Key Laboratory of Water Network Engineering and Scheduling of the Ministry of Water Resources and Southern Marine Science and Engineering Guangdong Laboratory (Zhuhai), School of Civil Engineering, Sun Yat-Sen University, Guangzhou, China

[2] Department of Land Surveying and Geo-Informatics, The Hong Kong Polytechnic University, Hong Kong, China

[3] School of Civil Engineering and Transportation, State Key Laboratory of Subtropical Building Science, South China University of Technology, Guangzhou, China

Published online: 09 March 2024

results at the seasonal timescale are consistent with that throughout the entire year except for winter. Overall, the results of this paper can help us to understand the possible causes of EPEs and serve in rainstorm forecasting and risk management at grid cell level for the whole of China.

1 Introduction

Extreme precipitation events (EPEs) have garnered considerable social concerns due to their hazardous and destructive nature (Visser et al. 2022). Associated with a wide array of natural hazards (Ali et al. 2021; Prein et al. 2017), EPEs can lead to substantial losses of life and inflict significant economic damages (Hoeppe 2016; Mahapatra et al. 2018). It is estimated that EPE-related hazards cause an annual financial loss of over 50 billion dollars and approximately 250,000 fatalities worldwide (Dube and Rao 2005; Min et al. 2011). In China, the Yangtze River basin was devastated by severe rainstorm floods in 1998, resulting in economic losses surpassing 22 billion dollars and claiming the lives of over 3000 individuals (Zhou et al. 2019). The flood season of 2016 witnessed 1192 counties being ravaged by rainstorm floods, incurring direct economic losses of approximately 20 billion dollars (Zhou et al. 2019). In July 2021, Henan Province experienced an extreme rainstorm disaster that impacted 14.814 million individuals, with a direct economic loss of about 18 billion dollars (Liu et al. 2023). The impacts of EPEs are particularly pronounced in countries like China owing to its vast geographical expanse, diverse topography and densely populated regions.

The occurrence of EPEs is influenced by thermodynamic and dynamic factors (Ali and Mishra 2018; Gorman 2012; Rudolph and Friedrich 2014). Focusing on the thermodynamic factors, responses of extreme precipitation to water vapor saturation pressure are investigated by using the theoretical relationship between temperature variation and water vapor saturation pressure (e.g. Formayer and Fritz 2017). Usually, the relationships between extreme precipitation and daily maximum temperature, daily mean temperature, as well as relative humidity are examined (Gao et al. 2020; Lepore et al. 2015; Loriaux et al. 2016). Considering the constraints imposed by water vapor availability and energy transport capacity, dynamic factors influence extreme precipitation through the modulation of large-scale circulation patterns, advection and atmospheric moisture content (Muller et al. 2011). For example, East Asian summer monsoon circulation, western Pacific subtropical high and El Niño-Southern Oscillation (ENSO) were observed to have considerable impacts on extreme precipitation in China (Chen 2013; Huang et al. 2003, 2022). Atmospheric instability, horizontal wind convergence and atmospheric moisture content were also considered (Chen 2013; Davies et al. 2013; Loriaux et al. 2016).

Crucial atmospheric conditions contributing to EPEs have been investigated (Li et al. 2023; Loriaux et al. 2016; Mishra et al. 2012). Focusing on the "21.7" Zhengzhou record-breaking precipitation event in China, investigations highlighted that synoptic-scale weather systems and land surface feedback were contributing factors to this remarkable event (Li et al. 2023; Wei et al. 2023). Moreover, the general relationships between EPEs and atmospheric conditions were also explored, and most of these studies only examined on an hourly scale or for selected events (Hardwick Jones et al. 2010; Mishra et al. 2012). Hardwick Jones et al. (2010) examined the scaling relationship between extreme precipitation and surface temperature in Australia, and found that the Clausius–Clapeyron (C–C) relationship only applies for individual storm systems. On the other hand, the possible causes of extreme precipitation were approached by systematically checking certain atmospheric conditions with correlation/regression methods (Xiong et al. 2023). For instance, the relationships between precipitation and atmospheric instability as well as temperature were quantified by regressions with the assumption that relationships between them are fixed (Lepore et al. 2016, 2015).

The complex and dynamic nature of precipitation and its relationships with atmospheric conditions necessitate a nuanced and flexible approach to accurately capture the underlying dynamics and spatial patterns (Chen and Hossain 2018; Loriaux et al. 2016). In this paper, the focus is concentrated on the relationships between EPEs in China and the atmospheric conditions of atmospheric instability, moisture availability and wind convergence, as well as the driving variables of vertical velocity, relative humidity and air temperature. The analysis is conducted by explicitly account for their coincidence probabilities, i.e., the ratio of the situations where precipitation and the given factor both reaching at extreme to the whole situations in EPEs (Chen and Hossain 2018; Rammig et al. 2015). The objectives of this paper are: (1) to quantify the controlling effects of atmospheric conditions and driving variables on EPEs, (2) to validate the atmospheric condition that dominantly controls EPEs in each grid cell, and (3) to identify the spatial patterns of the dominant controlling factors at annual and seasonal timescales. The insights into the relationships between EPEs and atmospheric conditions as well as driving variables are expected to contribute to rainstorm forecasting, environmental management and climate change adaptation.

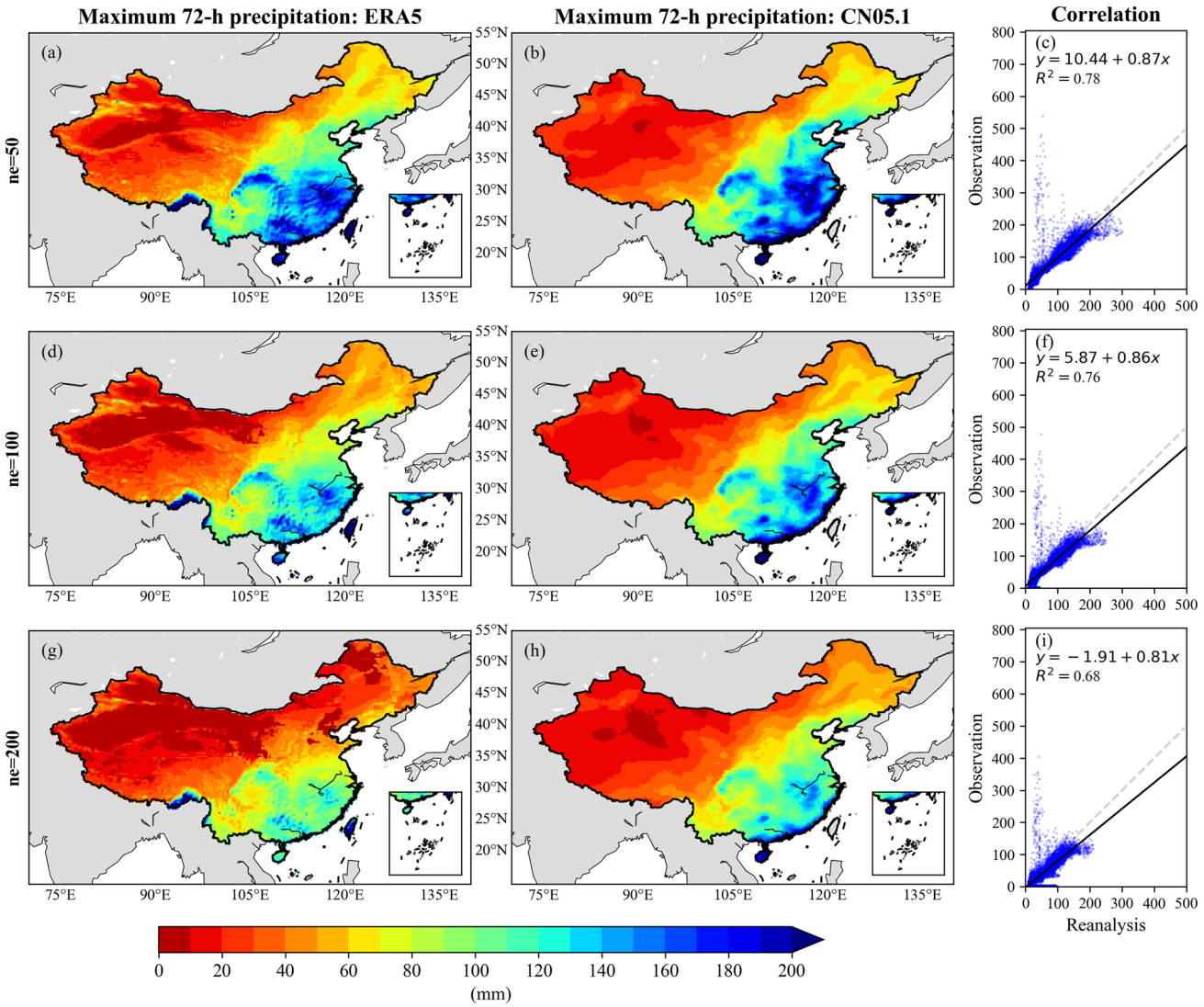

Fig. 1 Climatological maximum 72-h precipitation during 1968–2017 in ERA5 reanalysis (left) and CN05.1 observation (middle). The right column are the regressions between observation and reanalysis dataset, where the y axis is the CN05.1 observation and the x axis is the ERA5 reanalysis data. The numbers of EPEs are respective 50 in **a**–**c**, 100 in **d**–**f** and 200 in **g**–**i**

2 Data description

2.1 Reanalysis data

The fifth generation European Centre for Medium-Range Weather Forecasts atmospheric reanalysis (ERA5) (Hersbach et al. 2020) is used in this paper in order to illustrate the influence of atmospheric conditions and driving variables on EPEs. The data with latitude–longitude grid of 0.25° and temporal resolution of 1 h is used in the analysis. Precipitation and atmospheric conditions over 72-h durations are employed to address the time lag issue when quantifying the relationships between precipitation and various atmospheric conditions (Chen and Hossain 2018). This duration is also considered a standard design period for large water management infrastructures in practice, ensuring a comprehensive assessment of the relevant factors. The number of EPEs (ne) is set to be 50, 100 and 200 to examine the robustness of the findings. For each grid cell, the top 50/100/200 72-h precipitation events with the highest accumulated rainfall amount of reanalysis and observation datasets spanning from 1968 to 2017 (50 years) are extracted to assess the quality of the reconstructed precipitation climatology. The gridded observation dataset utilized in this paper is CN05.1 (Wu et al. 2017), which stands out as one of the most reliable observed datasets concerning air temperature and precipitation in China (Zhu et al. 2021).

The ERA5 climatological maximum 72-h precipitation (i.e., the top event) during 1968–2017 in comparison to

CN05.1 is shown in Fig. 1. The two products are generally in accordance with each other. The maximum 72-h precipitation consistently decreases from southeast to northwest. The right column of Fig. 1 shows the correlation between the maximum 72-h precipitation in ERA5 and CN05.1. The coefficients of the linear regression slightly decrease with the increase of the number of EPEs. Overall, precipitation data of ERA5 shows a high correlation with the observations. Atmospheric variables of ERA5 have been employed in several regions around the world to conduct analyses (Betts et al. 2019; Urraca et al. 2018), as a standard or comparation object for evaluation of the datasets (Li et al. 2021; Shen et al. 2022; Yang et al. 2022). These results indicate that the ERA5 data is suitable for analyzing the relationships between EPEs and related atmospheric conditions as well as driving variables in China.

2.2 Atmospheric conditions

Atmospheric conditions represent the state of the atmosphere in terms of instability, moisture availability and moisture convergence. Convective available potential energy (CAPE), precipitable water (PW) and vertical velocity at 700 hPa (verV) respectively represent atmospheric instability, moisture availability and moisture convergence (Chen and Hossain 2018), which are considered to be influential contributors to EPEs (Davies et al. 2013; Gao et al. 2020; Hardwick Jones et al. 2010).

The CAPE serves as a valuable indicator of atmospheric instability, providing insights into the potential for the development of convection, which often leads to heavy rainfall, thunderstorms and other severe weather phenomena (Hersbach et al. 2023a). It plays a crucial role in the accurate prediction of severe weather events (Brooks et al. 2003). Higher value of CAPE indicates a more unstable atmosphere and a greater potential for severe weather. In thunderstorm environments, observed CAPE values often exceed 1000 J kg^{-1}, and in extreme cases, they can even surpass 5000 J kg^{-1} (Hersbach et al. 2023a).

The PW refers to the total amount of water vapor present in a column extending from the Earth's surface to the top of the atmosphere (Hersbach et al. 2023a), which indicates the moisture available for rainstorms. During intense rainstorm events, the amount of moisture depleted can be several times greater than the precipitable water content.

The vertical velocity refers to the speed of air motion between different pressure levels. It provides valuable understandings into the large-scale dynamics of the atmosphere. The strength of vertical velocity is also an approximation of the large-scale horizontal convergence (LSC) from the mass balance perspective (Hersbach et al. 2023b). It helps us understand the overall atmospheric dynamics and the convergence of air masses on a larger scale. It was shown that a significant amount of water vapor enters the rainstorm system at lower levels, typically below 3000 m (Loriaux et al. 2016; Zhan and Ye 2000). Vertical velocity at 700 hPa and 850 hPa have been investigated in previous studies (Loriaux et al. 2016; McErlich et al. 2023). Two different layers of variables are both examined in the analysis and comparison of the results are shown in the supplementary material (Figures S1 and S2). Therefore, vertical velocity at 700 hPa is chosen as it is more relevant to precipitation processes (Chen and Hossain 2018).

2.3 Driving variables

Driving variables in this paper serve as the fundamental atmospheric variables that have driving effects on the aforementioned atmospheric conditions and the 72-h extreme precipitation process, i.e., vertical velocity, relative humidity and air temperature. Specifically, the four relatively independent variables selected are as follows: verV, relative humidity at 700 hPa (RH), average air temperature between 850 and 500 hPa (Tavg) as well as air temperature difference between 850 and 500 hPa (Tdiff) (Chen and Hossain 2018). The inclusion of verV in the analysis of driving variables is motivated by its ability to not only indicate water vapor convergence but also influence the moisture and stability of the atmosphere. The variables RH and Tdiff are closely related to the components included in K-index, which was originally used for assessing the likelihood of thunderstorms to occur that incorporates both stability and moisture (Charba 1977). The high values of K-index are typically observed when the atmosphere is characterized by high levels of moisture and instability, particularly with significant low-level moisture. Relative humidity measures the proximity to atmospheric saturation. Like vertical velocity, comparisons of the results between 700 and 850 hPa are presented in Figures S1 and S2. Although relative humidity at 850 hPa is slightly more relevant to EPEs, it has a little effect on the identification of dominant controlling factors comparing to vertical velocity. Therefore, like verV, relative humidity at 700 hPa is selected. This selection aligns with the midlevel relative humidity term within K-index. Similarly, Tdiff which represents the vertical temperature lapse rate, is a relevant component within K-index.

3 Research methods

3.1 Definition of precipitation events

The precipitation threshold (*PT*) and dry interval (*DI*) are employed to distinguish between precipitation events (Gaál et al. 2014; Loriaux et al. 2016; Molnar et al. 2015). Considering the characteristics of the ERA5 reanalysis precipitation

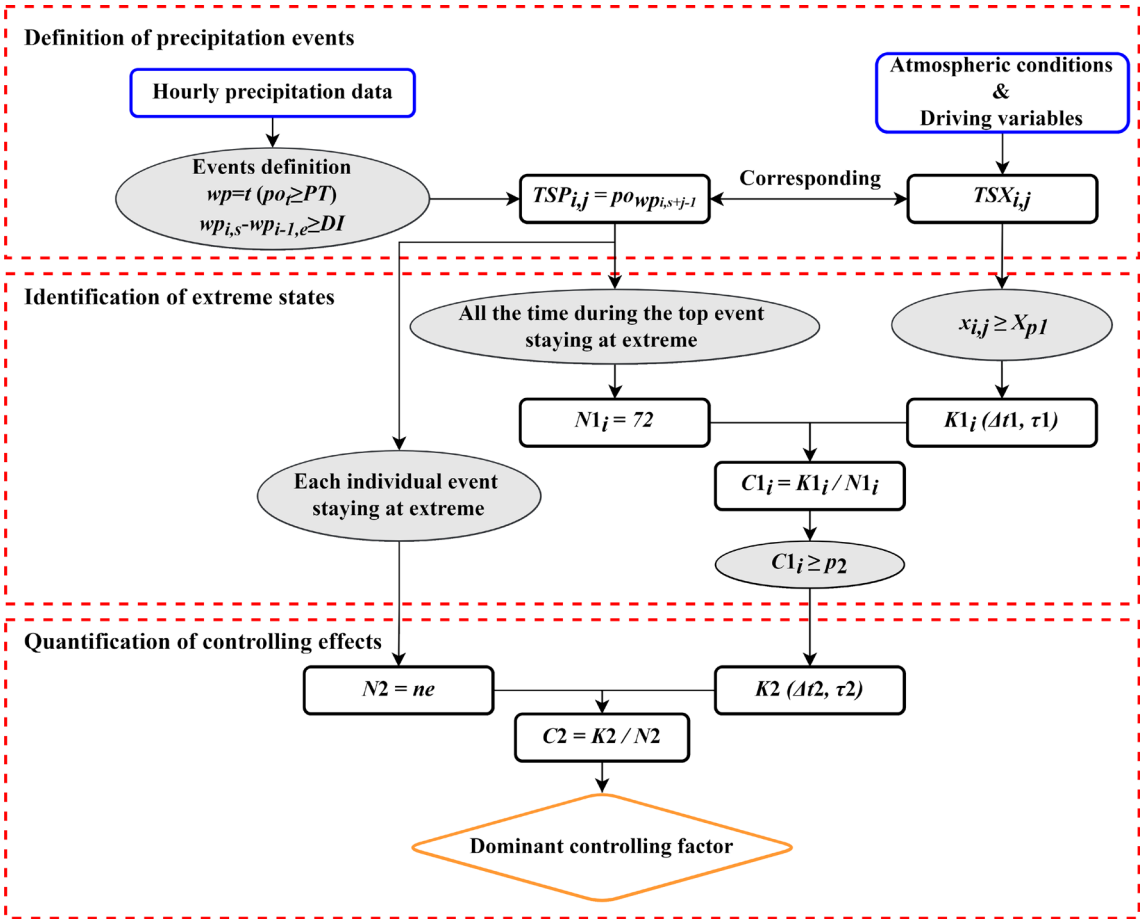

Fig. 2 Procedure of the method relating EPEs to atmospheric conditions and driving variables

data and observations used in this paper for the Chinese region, a *PT* of 0.1 mm and a *DI* of 6 h are utilized (the results of sensitivity tests in Figures S3 and S4 indicate that *PT* = 0.1/0.5 and *DI* = 2/6/10 have marginal effects on the identification of dominant controlling factors):

$$wp = t\,(po_t \geq PT), \tag{1}$$

$$wp_{i,s} - wp_{i-1,e} \geq DI, \tag{2}$$

$$TSP_{i,j} = po_{wpi,s+j-1}, \tag{3}$$

where *wp* indicates wet periods, *t* indicates the time order in the hourly data, *po* indicates the hourly precipitation data, *i* indicates each top event ($i = 1,\ldots,$ne), *s* indicates the start time in a precipitation event, *e* indicates the end time in a precipitation event, *TSP* indicates time series of precipitation events, *j* indicates each hour during the 72-h event ($j = 1,\ldots,72$). Overall, adjusting these parameters has minimal impact on the results. Although this method may be rough and arbitrary, it proves to be effective in preventing the double counting of extreme rainfall amounts within the same event. In this paper, the top 50/100/200 72-h precipitation events and corresponding factors with the highest cumulative 72-h rainfall amount at every grid cell over a span of 50 years are identified and extracted:

$$TSP_{i,j} \rightarrow TSX_{i,j}, \tag{4}$$

where *TSX* indicates time series of factor X, i.e., CAPE, PW, verV, RH, Tavg and Tdiff.

There are three steps to examine the relationships between EPEs and atmospheric conditions as well as driving variables, as shown in Fig. 2. The method relating EPEs to atmospheric conditions and driving variables is based on the classic coincidence probability. The classic coincidence probability was originally proposed by Donges et al. (2011) in a different context, searching for both instantaneous and lagged coincidences between specific percentiles in the pair of time series. To determine the number of coincidences (*K*) between two given time series, situations where both two time series exhibit extreme state simultaneously or with a predefined time lag are identified. The parameters used in this analysis are as follows: (1) Δt, which determines the

width of the time window, ensuring that only coincidences within this window are considered, and (2) τ, which represents the time lag. A τ value of 0 signifies instantaneous coincidences, where both events occur simultaneously (Rammig et al. 2015). To normalize K, the total number of coincidences is divided by the number of extreme situations (N) in the time series. This normalization allows us to obtain the coincidence probability (C), which ranges between 0 and 1. A value of 0 indicates no coincidences, while a value of 1 signifies the maximum number of possible coincidences. The classic coincidence probability serves as an index, indicating the extent to which the given factor influences the occurrence of 72-h EPEs at a specific grid cell.

3.2 Identification of extreme states

At each grid cell, the cumulative distribution function (CDF) for the atmospheric conditions and driving variables using climate records in the period from 1968 to 2017 are calculated. For determination of extreme state, CDF = 95% (referred to as parameter p_1) is considered as the threshold. Whether the factor X, i.e., CAPE, PW, verV, RH, Tavg and Tdiff, representing the entire individual event i is in an extreme state depends on the coincidence probability for intra-event ($C1_i$). Assuming that hourly rainfall amount stays at extreme all the time during the top event in the analysis, the number of extreme situations is set to be 72 for each event ($N1_i = 72$). Therefore, during each top event, the situations where factor X stays at extreme are also the situations where both two time series exhibit extreme state. The number of coincidences within an individual event, $K1_i$, determined by $\Delta t1 = 1$ h, $\tau 1 = 0$, is simply calculated as:

$$k1_{i,j} = \begin{cases} 1, \ if \ x_{i,j} \geq X_{p_1} \\ 0, \ otherwise \end{cases}, \tag{5}$$

$$K1_i(\Delta t1, \tau 1) = \sum_{j=1}^{72} k1_{i,j}, \tag{6}$$

where $k1_{i,j}$ indicates that if the factor X stays at extreme for hour j during the event i, $x_{i,j}$ indicates the factor X value for hour j during the event i, X_{p_1} indicates the factor X value at CDF of p_1. The coincidence probability for intra-event is calculated as:

$$C1_i = \frac{K1_i}{N1_i}. \tag{7}$$

If coincidence probability for intra-event between precipitation and factor X exceeds 15% (parameter p_2) during the 72-h duration, factor X representing the event i is identified to reach an extreme state.

3.3 Quantification of controlling effects

The coincidence probability for multi-event ($C2$) is used to quantify the controlling effects of atmospheric conditions and driving variables on EPEs. Considering each individual extreme precipitation event to be in an extreme state indicates that $N2 = 50/100/200$ events. The number of coincidences for multi-event, $K2$, determined by $\Delta t2 = 1$ event, $\tau 2 = 0$, is simply calculated as:

$$k2_i = \begin{cases} 1, \ if \ C1_i \geq p_2 \\ 0, \ otherwise \end{cases}, \tag{8}$$

$$K2\,(\Delta t2, \tau 2) = \sum_{i=1}^{ne} k2_i, \tag{9}$$

where $k2_i$ indicates that if the factor X representing the entire individual event i is in an extreme state. The coincidence probability for multi-event, is calculated as:

$$C2 = \frac{K2}{N2}, \tag{10}$$

which also illustrates the percentage of the EPEs that are related to extreme atmospheric conditions and driving variables. Assuming that the factor exhibiting the highest coincidence probability influences EPEs most, the dominant controlling factor of EPEs is identified (Chen and Hossain 2018). Based on the complete records spanning from 1968 to 2017, these analyses allow for the derivation of dominant controlling factors throughout the year and across seasons.

4 Results

4.1 Results at the annual timescale

There are considerable spatial variations of coincidence probabilities between EPEs and extreme CAPE, PW, verV, RH, Tavg as well as Tdiff during 1968–2017 at the annual timescale, as shown in Fig. 3. Irrespective of the ne set to be 50, 100 or 200, the spatial distributions of coincidence probabilities remain largely consistent across all factors. These findings indicate the stability of the results.

The CAPE exhibits higher coincidence probabilities in Northwest China (Fig. 3a–c), suggesting a stronger influence of CAPE on EPEs in this region compared to other areas. Additionally, the mean annual CAPE values are found to be higher in Southeast China and lower in Northwest China, further reinforcing the credibility of the observation that CAPE exerts significant control in Northwest China. Notably, the coincidence probability values for CAPE are comparatively lower in the Tianshan Mountains, Kunlun

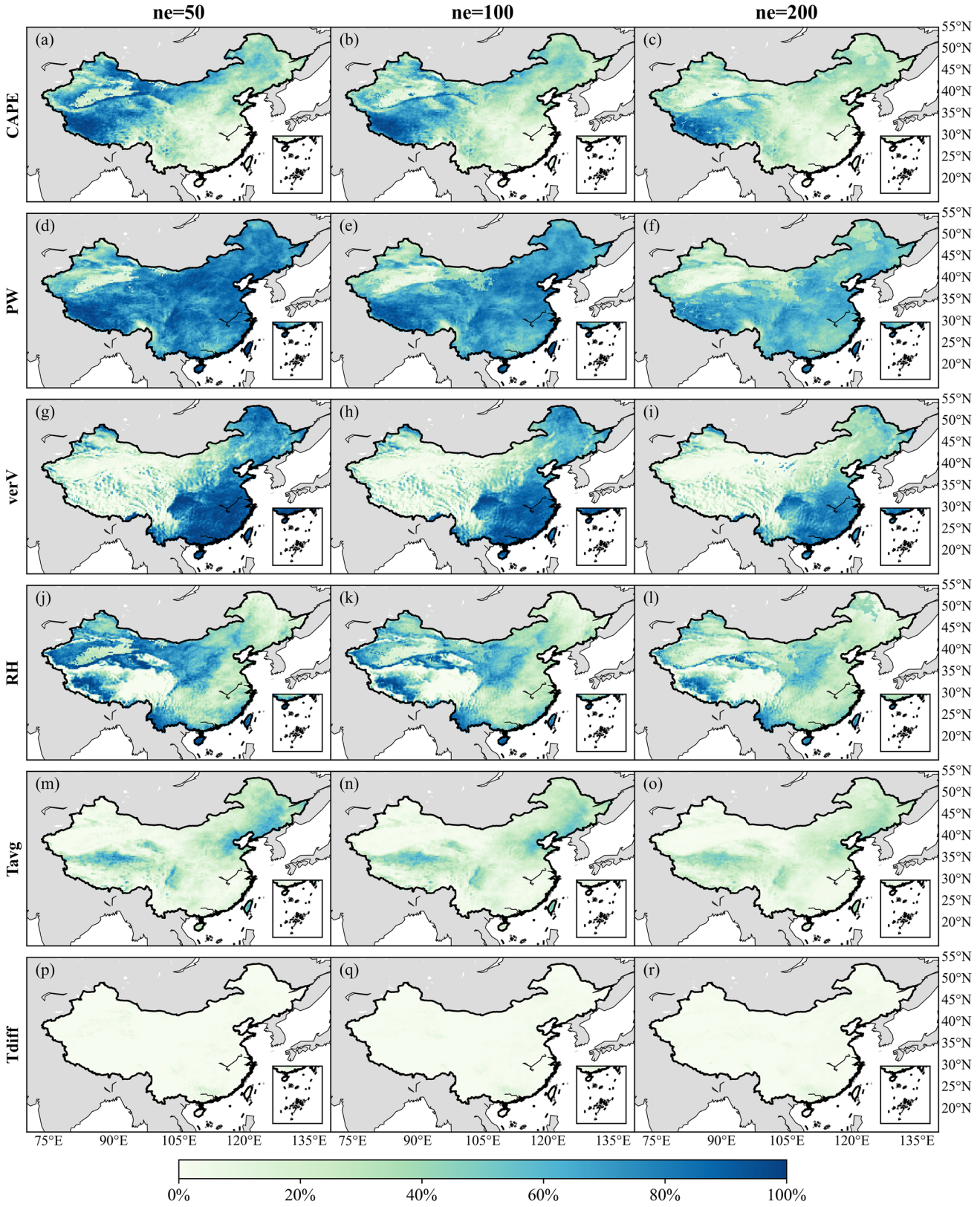

Fig. 3 The coincidence probabilities between EPEs and extreme **a–c** CAPE, **d–f** PW, **g–i** verV, **j–l** RH, **m–o** Tavg and **p–r** Tdiff during 1968–2017 at the annual timescale. The numbers of EPEs are respective 50 (left), 100 (middle) and 200 (right)

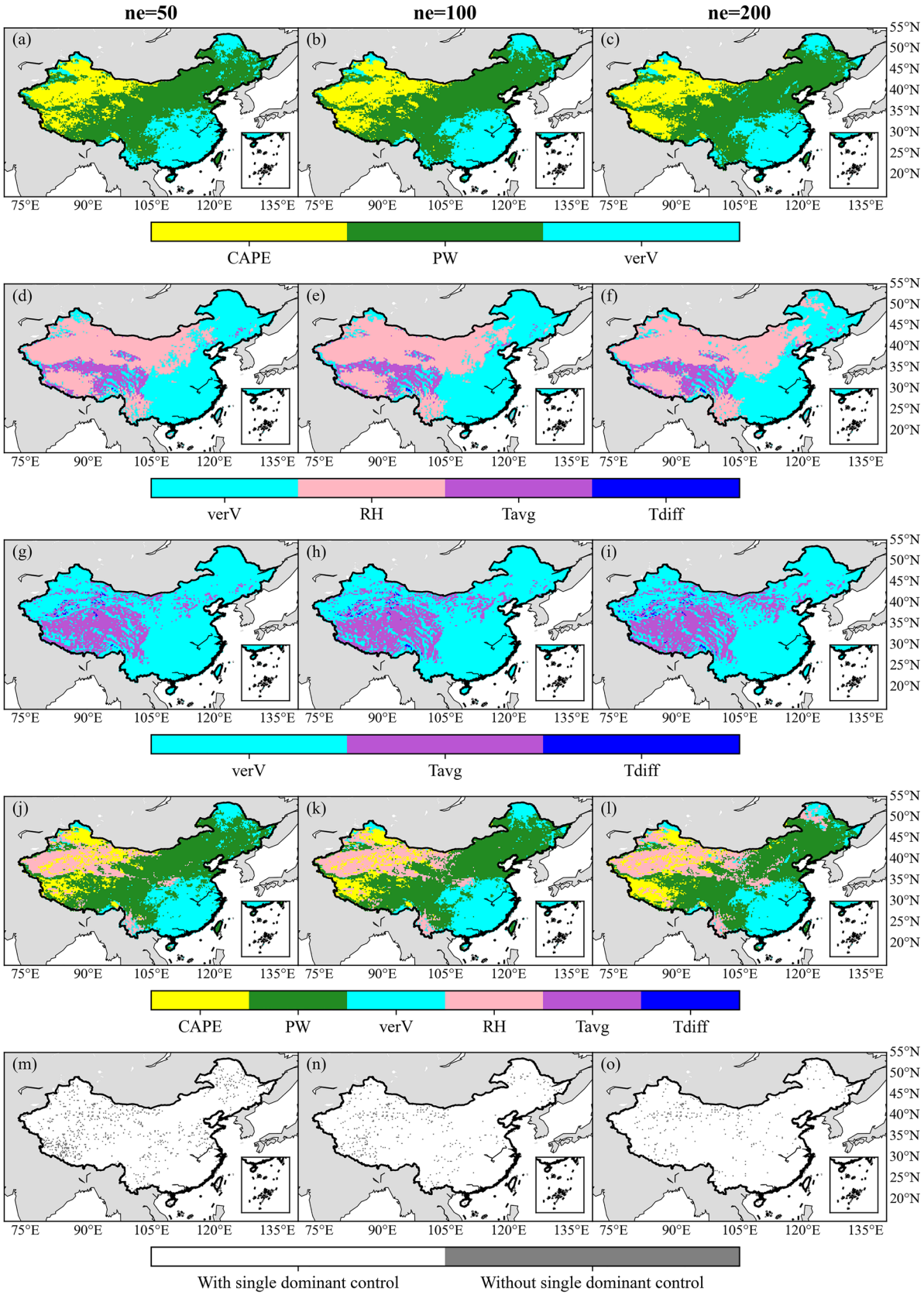
ne=50
ne=100
ne=200
(a)
(b)
(c)
(d)
(e)
(f)
(g)
(h)
(i)
(j)
(k)
(l)
(m)
(n)
(o)
75°E
90°E
105°E
120°E
135°E
55°N
50°N
45°N
40°N
35°N
30°N
25°N
20°N
CAPE
PW
verV
RH
Tavg
Tdiff
With single dominant control
Without single dominant control

◂**Fig. 4** Dominant controlling factors of EPEs at the annual timescale for analyses using **a–c** CAPE/PW/verV, **d–f** verV/RH/Tavg/Tdiff, **g–i** verV/Tavg/Tdiff and **j–l** CAPE/PW/verV/RH/Tavg/Tdiff. And **m–o** reflect if the grid cell has the single dominant controlling factor or not. The numbers of EPEs are respective 50 (left), 100 (middle) and 200 (right)

Mountains, Qilian Mountains and southeastern Qinghai-Tibet Plateau regions.

The PW displays a consistently high level of coincidence probability values across the entire country (Fig. 3d–f), which aligns with the widely accepted notion that water vapor supply plays a crucial role in precipitation formation. However, it is worth noting that the coincidence probability values for PW are slightly lower in Xinjiang and the southeastern Qinghai-Tibet Plateau regions.

The verV presents a regional complementarity of coincidence probabilities with that of CAPE (Fig. 3g–i), indicating a strong control effect on EPEs in Southeast China. The verV demonstrates high values in southern region of the Yunnan-Guizhou Plateau and southeastern boundary of the Qinghai-Tibet Plateau, specifically at the junction of the Himalayas and Hengduan Mountains. This pattern may be associated with the influence of the southwest monsoon from Indian Ocean. Furthermore, it is interesting to observe that the coincidence probability values for verV are higher in the vicinity of the Tianshan Mountains and the Altai Mountains, which differs from the phenomenon that the values are lower in Northwest China.

The RH has higher coincidence probability values in Northwest China (Fig. 3j–l), but lower in eastern part of the Qinghai-Tibet Plateau. Ignoring the absolute value, the distribution pattern of coincidence probability is similar to that of CAPE, where the coincidence probability values for RH in the Tianshan, Kunlun and Qilian Mountains are lower compared to the nearby regions.

The Tavg (Fig. 3m–o) and Tdiff (Fig. 3p–r) generally have low coincidence probability values across the entire country. However, it is noteworthy that the coincidence probability values for Tavg are higher in specific regions such as the Kunlun Mountains, Qilian Mountains, Sichuan Basin, Changbai Mountains, Northeast Plain and northern North China Plain.

The CAPE, PW and RH all demonstrate high coincidence probabilities in Northwest China, warranting further examination at a sub-regional level. For instance, these three factors exhibit differences between northern and southern Xinjiang. Using the Tianshan Mountains as a boundary, the coincidence probability values for RH in the Junggar Basin are slightly lower compared to those in southern Xinjiang. On the Inner Mongolia Plateau, the coincidence probability values for PW are notably higher than those for CAPE and RH. In Qinghai, the areas with high coincidence probability values decrease in the order of PW, CAPE and RH. In southeastern boundary of the Qinghai-Tibet Plateau, the coincidence probability values for CAPE, PW and RH are low, potentially influenced by water vapor transported by the southwest monsoon from Indian Ocean. Surprisingly, the coincidence probability values for verV are higher in this area instead.

The PW is influenced by two driving variables: Tavg, representing the maximum moisture holding capacity, and RH, which indicates the proximity of actual air moisture to the maximum capacity (Chen and Hossain 2018). However, the coincidence probability values for Tavg tend to be low, suggesting that Tavg may not be a primary factor driving PW to extreme in precipitation.

Based on the findings depicted in Fig. 3, a single dominant controlling factor that exerts the most influence on 72-h EPEs at each grid cell can be identified (Fig. 4). The "competition" among atmospheric conditions at the annual timescale is shown in Fig. 4a–c. Generally, Southeast and Southwest China are dominantly controlled by verV, North and Central China by PW and Northwest China by CAPE.

Southeast and Southwest China as well as part of Northeast China are dominantly controlled by verV, most of which are wet regions according to the dry/wet classification of areas (typically with mean annual precipitation limits of 800, 400 and 200 mm). In these areas, water vapor is mainly transported by the southeast monsoon from Pacific Ocean, while southeastern boundary of the Qinghai-Tibet Plateau is influenced by the southwest monsoon from Indian Ocean. These regions typically have ample water vapor supply, and moisture convergence contributes to moisture transport from nearby areas. In the case of EPEs, the water vapor consumed is several times that PW. Hence, verV plays a more crucial role in controlling EPEs in these regions. However, there are exceptions where PW or even CAPE take precedence in the wet regions. For instance, PW controls EPEs in the Changbai Mountains, Taiwan Mountains, southwestern Hainan, Wushan Mountains and Yunnan-Guizhou Plateau, which are characterized by mountainous and plateau terrains. In these areas, water vapor is lifted by the topography, making sufficient moisture crucial for EPEs. In the southeastern corner of Tibet, specifically at the junction of the Himalayas and Hengduan Mountains, the higher terrain and lower temperatures create a colder and more stable air mass. As a result, significant disturbance in the form of CAPE is required to trigger extreme precipitation in these regions.

Part of Northeast China, North and Central China, part of the Qinghai-Tibet Plateau, as well as the areas near by the Tianshan Mountains are dominantly controlled by PW, which mostly consist of semi-humid and semi-arid regions. However, in certain mountainous areas with sufficient water vapor, verV replaces PW as the dominant controlling factor even though they belong to semi-humid and semi-arid

regions. This is observed in the northern Tianshan Mountains and the Altai Mountains. In the northwestern Junggar Basin, there is a topographic gap where prevailing westerly winds can transport water vapor from the North Atlantic. Despite the considerable distance, the westerly winds pass through the flat Western European plain, Eastern European plain and low Kazak hills, encountering less obstruction in reaching this area. Along with that from the Arctic Ocean, water vapor is influenced by the uplifting effect of the Tianshan Mountains. Similarly, water vapor from North Atlantic, carried by prevailing westerly winds, is uplifted over the Altai Mountains. In these regions, verV plays a crucial role in generating EPEs. Additionally, in areas with higher terrains, such as the western Qinghai-Tibet Plateau, CAPE becomes the dominant controlling factor due to the cold and stable air condition although they are semi-humid and semi-arid regions.

Northwest China are dominantly controlled by CAPE, the majority of which are arid regions characterized by dry, hot climate and stable air condition. In comparison to other regions, these areas experience lower level of extreme rainfall, requiring less water vapor for precipitation. Furthermore, the conversion efficiency of PW to precipitation is relatively high in Northwest China (Dong et al. 2019). Therefore, in the presence of significant disturbances, EPEs may occur in these regions. However, the Qaidam Basin, despite being part of arid areas, is dominantly controlled by PW, which is low lying, surrounded by plateau mountains and has slightly lower temperature than nearby areas.

The "competition" among driving variables at the annual timescale (Fig. 4d–f) reveal that RH plays a driving role in Northwest China and Inner Mongolia Plateau, while verV takes precedence in Southeast China, and Tavg has a considerable impact on a small portion of the Qinghai-Tibet Plateau. The notable influence of RH can be attributed to its inherent upper limit, with values typically capped at 100% (or exceeding 100% in supersaturation conditions). RH often persists near this upper bound during EPEs. Additionally, RH tends to reach its annual maximum in winter, when it is more challenging for other factors to reach extreme state. For these reasons, another evaluation excluding RH is performed, and the results are illustrated in Fig. 4g–i. The findings indicate that verV drives extreme precipitation in most parts of the country, while Tavg takes over as the primary factor in the Qinghai-Tibet Plateau.

The comprehensive comparisons of atmospheric conditions and driving variables at the annual timescale are provided in Fig. 4j–l. The spatial distribution patterns observed in Fig. 4j–l are similar to that in Fig. 4a–c, indicating the stability of the dominant controlling factors. It confirms that the driving variables affect extreme precipitation by driving CAPE, PW and verV to extreme state. The individual effect does not surpass the impact of the dominant controlling atmospheric condition itself. It should be noted that some grid cells controlled by RH may be influenced by its natural upper limit. The significance of the dominant controlling factor for a single grid cell is examined (Fig. 4m–o). If the grid cell has one single dominant control (i.e., one single highest coincidence probability value), the result is considered to be significant. And it is confirmed that in the majority of areas in China, the method of determining the dominant controlling factors of EPEs by using the classic coincidence probabilities is shown to be effective.

4.2 Results at the seasonal timescale

The seasonal variations in the coincidence probabilities between EPEs and extreme CAPE, PW, verV, RH, Tavg as well as Tdiff are shown in Fig. 5, and top fifty EPEs during the selected season are chosen.

The coincidence probabilities are low during December–January–February (DJF), which could be attributed to the relatively reduced occurrence of extreme precipitation in China during that season. Results demonstrate that CAPE exhibits relatively low coincidence probability values during June–July–August (JJA) and governs a smaller geographical area (Fig. 5b). Furthermore, RH displays higher coincidence probability values in Southeast China during JJA compared to the rest of the year (Fig. 5n). In terms of other factors, the spatial distributions of coincidence probabilities in March–April–May (MAM), JJA and September–October–November (SON) closely resemble those observed throughout the entire year.

The seasonal variations in the dominant controlling factors are presented in Fig. 6. Similarly, due to the relatively lower occurrence of extreme precipitation in China during DJF, there is no evident spatial pattern of the dominant controlling factors during that season. PW occupies more dominant regions than that controlled by CAPE and verV in MAM (Fig. 6a). During JJA, verV and PW control larger areas in Northeast and Northwest China respectively (Fig. 6b). Additionally, Tavg controls a smaller region compared to other factors in JJA (Fig. 6f). The distributions of "competition" among atmospheric conditions and driving variables in MAM, JJA and SON exhibit similar patterns that observed throughout the entire year. These findings simplify the practical application of results and signify the stability of the dominant controlling factors.

4.3 Results by region

Three case study regions are selected to delve into the relationships between EPEs and atmospheric conditions as well as driving variables. Being different from the above analysis at the grid cell level, the area-weighted data is used (Loikith et al. 2017; Thompson et al. 2020). The precipitation time

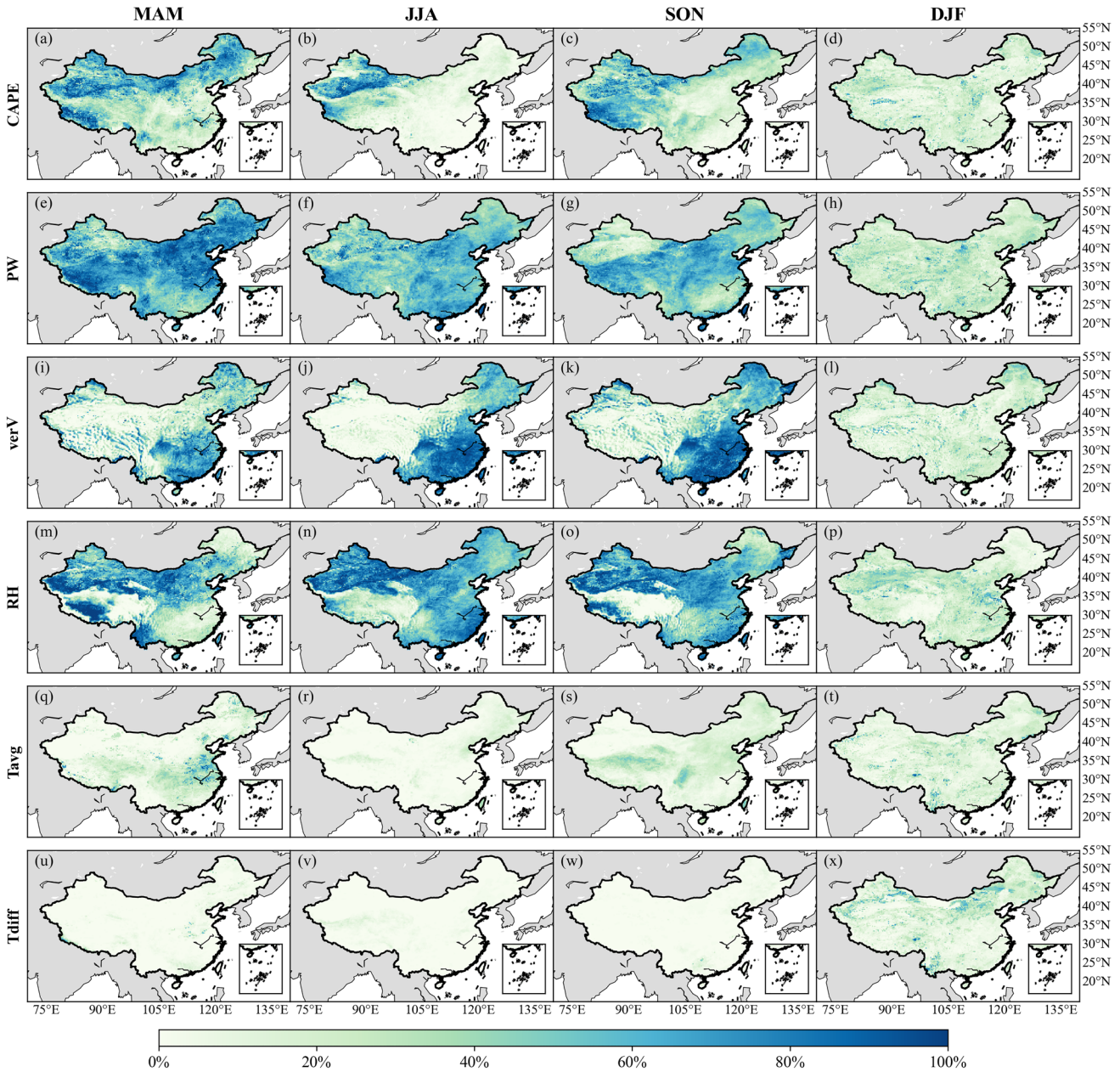

Fig. 5 Seasonal variations in the coincidence probabilities between EPEs and extreme **a–d** CAPE, **e–h** PW, **i–l** verV, **m–p** RH, **q–t** Tavg and **u–x** Tdiff during 1968–2017

series from ERA5 and the top fifty 72-h precipitation events with the highest rainfall amount during 1968–2017 of Urumqi, Beijing and Guangzhou regions are shown in Fig. 7. Urumqi region is in the middle temperate zone of the continental arid climate, characterized by a dry climate throughout the year, rare precipitation and significant temperature variations between day and night (Zheng et al. 2010). The maximum rainfall event occurred on June 8th, 1978, starting at 23:00, with a cumulative rainfall amount of 50.8 mm approximately. Beijing region is situated in the warm temperate sub-humid continental monsoon climate zone, characterized by hot and rainy summers as well as cold and dry winters (Zheng et al. 2010). In the analysis, the maximum rainfall event in Beijing began at 18:00 on July 18th, 2016, accumulating 173.7 mm of rainfall amount approximately. Guangzhou region falls within the subtropical monsoon climate zone, characterized by hot and humid summers and mild and dry winters (Zheng et al. 2010). From 1968 to 2017, all the top fifty 72-h precipitation events in Guangzhou region record cumulative rainfall amounts exceeding 100 mm. The maximum rainfall event took place on May

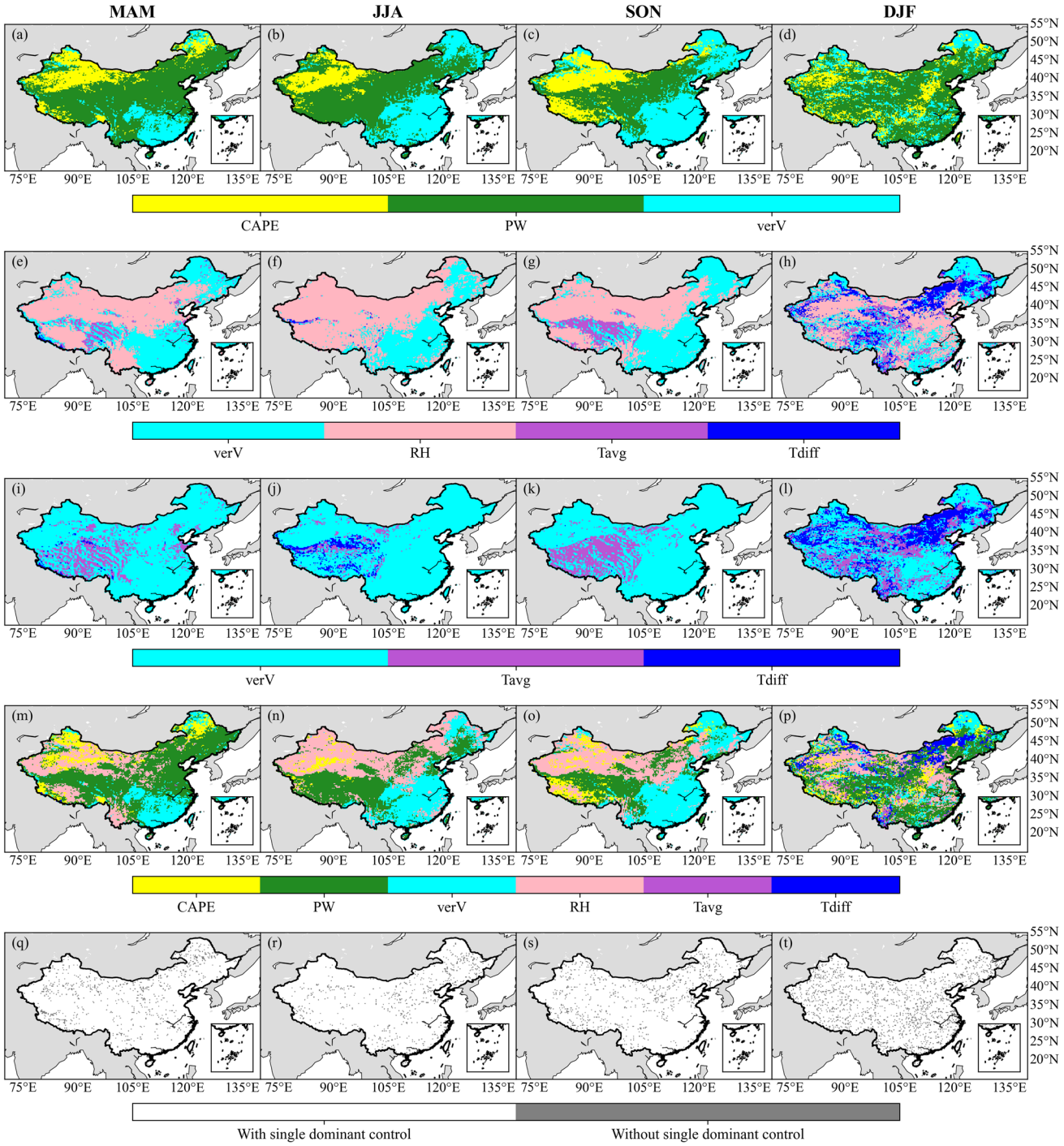

Fig. 6 Seasonal variations in the dominant controlling factors: **a–d** CAPE/PW/verV, **e–h** verV/RH/Tavg/Tdiff, **i–l** verV/Tavg/Tdiff, **m–p** CAPE/PW/verV/RH/Tavg/Tdiff. And **q–t** reflect if the grid cell has the single dominant controlling factor or not

24th, 2008, starting at about 9:00, resulting in a cumulative rainfall amount of approximately 314.3 mm.

For the maximum 72-h precipitation event with the highest rainfall amount, the temporal evolution of rainfall, atmospheric conditions and driving variables are shown in Fig. 8. RH reached at extreme for 51 h, followed by verV in Urumqi region. These two factors played crucial roles in controlling this event, but CAPE emerges as the dominant controlling factor of EPEs in Urumqi region on the basis of the analysis among the top fifty events. In Beijing region, PW consistently reached at extreme within the 72-h period with the $C1_1$ value of 1 and PW is also the dominant controlling factor

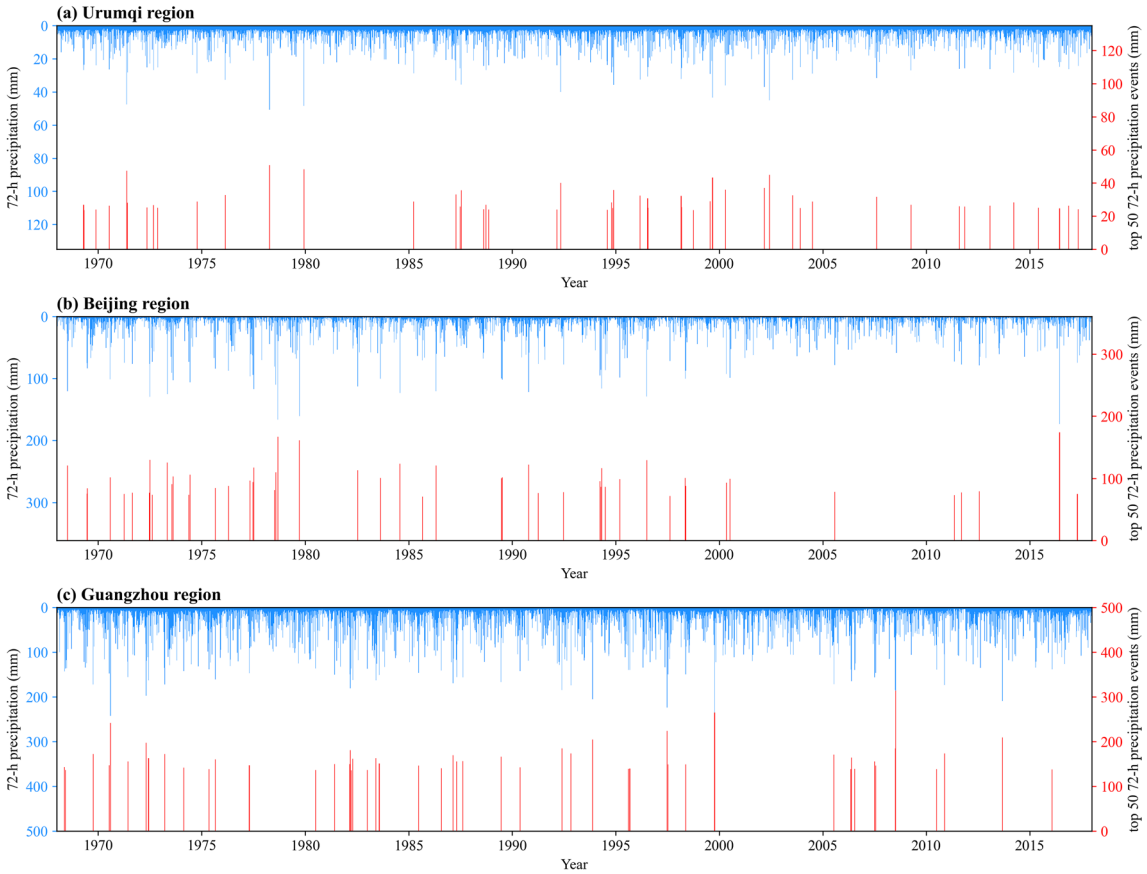

Fig. 7 The precipitation time series from the reanalysis and the top fifty 72-h precipitation events with the highest rainfall amount during 1968–2017 of **a** Urumqi region, **b** Beijing region and **c** Guangzhou region

of EPEs. Following PW, Tavg, verV and RH exhibited high values and played notable roles in controlling this event. In Guangzhou region, PW reached at extreme for 64 h, ranking first in terms of $C1_1$, followed by verV, RH and Tavg. Although PW had the highest $C1_1$ value in this event, the coincidence probability values for verV were higher among the top fifty EPEs, indicating that verV serves as the dominant controlling factor of EPEs in Guangzhou region. Notably, the temporal evolution of verV closely resembled that of rainfall in all these regions.

The CDF curves of CAPE, PW, verV, RH, Tavg and Tdiff, which are derived from climate records in the period from 1968 to 2017, are shown by the blue lines in Fig. 9. The values of atmospheric conditions and driving variables for the maximum 72-h precipitation event are overlaid with the CDF curves, indicated by red dots. The CDF curves of CAPE and PW in Urumqi region are quite different from that in Beijing region and Guangzhou region. CAPE in Urumqi region tends to remain at a low state, with even the value at the 95th percentile on the CDF being relatively low, not reaching 1000 J kg^{-1} that often observed in thunderstorm environments. For PW in Urumqi region, the value at 95th percentile is about 20 mm which is below half that of other two regions. This phenomenon may be attributed to the lower absolute values of total rainfall amount typically observed in arid regions like Urumqi.

5 Discussion

The classic coincidence probability has been utilized to investigate the controlling factors of extreme precipitation for United States (Chen and Hossain 2018) and also for Henan Province in China (Lang et al. 2022). The investigations conducted by Chen and Hossain (2018, 2019) highlighted the spatial variations of the controlling factors and emphasized the significance of verV in the continental United States. These findings opened up new avenues for statistical analyses and the development of hybrid models in estimating probable maximum precipitation (PMP). Lang et al. (2022) suggested that verV and PW are the dominant controlling factors during summer, while CAPE and verV exhibit a strong relation to EPEs during winter in Henan. When examining the seasonal variation, it is important to note that Lang et al. (2022) identified the EPEs that took

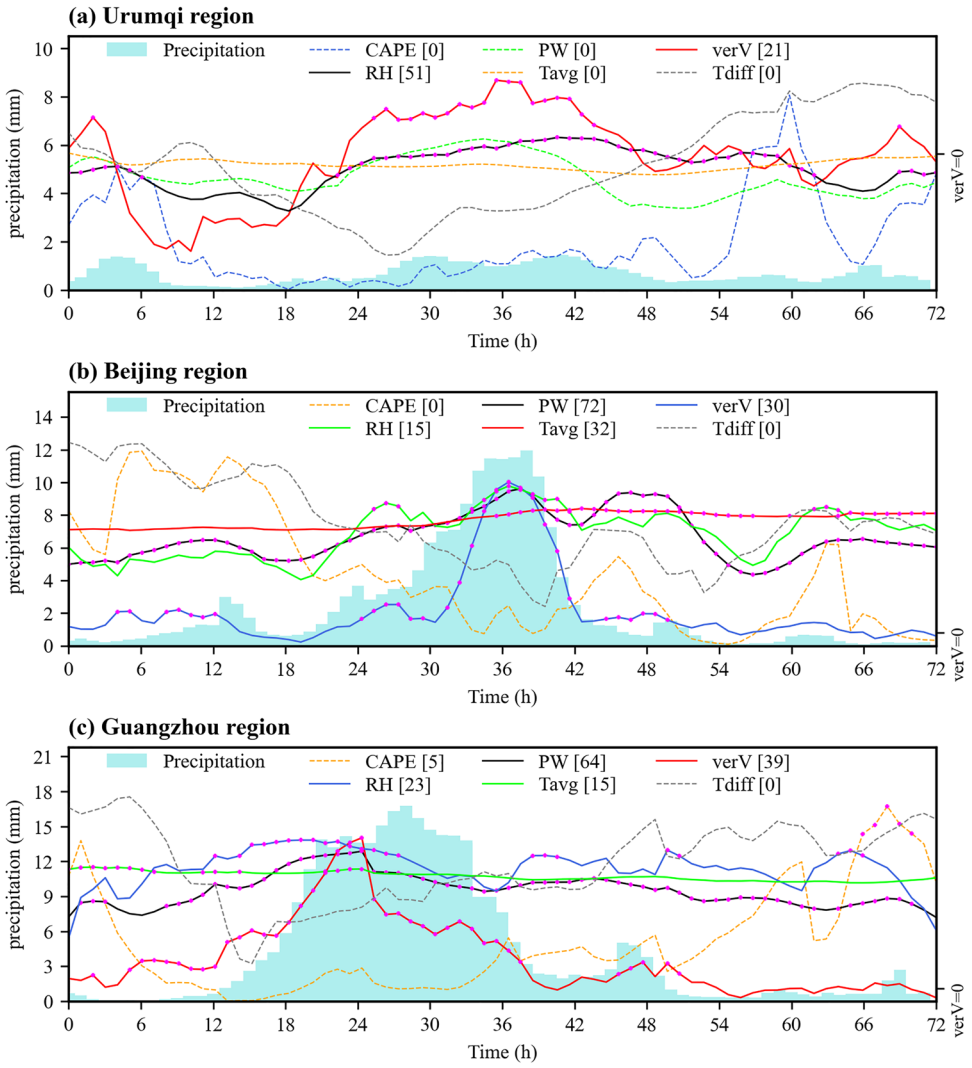

Fig. 8 Temporal evolution of the rainfall, atmospheric conditions and driving variables for the maximum 72-h precipitation event in **a** Urumqi region, **b** Beijing region and **c** Guangzhou region. The number in "[]" reflects how many hours that the factor stays extreme (marked with purple dots) during the selected 72-h rainstorm event. The color of the line indicates the number of periods in which the factor stays extreme, with black, red, blue, green, orange and grey representing from the highest to the lowest periods respectively. And the dashed line indicates that the factor does not control this event

place throughout the year and categorized them into seasons according to their occurrence time. In contrast, this paper selects the top fifty EPEs within each season. As a result, there may be discrepancies in the seasonal distributions of coincidence probabilities. Nonetheless, the findings regarding the dominant controlling factors remain largely consistent. Although the key atmospheric conditions and driving variables contributing to EPEs are investigated while considering spatial patterns, there is still a need for a localized investigation to obtain even more reliable results.

Environmental conditions contributing to long-term variations can also affect the spatial patterns and classification of EPEs (Cipolla et al. 2020), such as topography (Li et al. 2019; Vanden Broucke et al. 2019), monsoonal circulation systems (Zhu et al. 2011) and also urbanization-induced heat island and aerosol effects (Zhong et al. 2015). In China, the large scale environmental conditions such as East Asian monsoon, western Pacific subtropical high, mid-latitude disturbances (Huang et al. 2003) and westerly winds in the South China Sea caused by the Madden–Julian Oscillation (MJO) (Tao and Wei 2007) have been taken into account to analyze the formation mechanisms of EPEs. On the Qinghai-Tibet Plateau, the connection between winter snow cover with the occurrence of EPEs in South China was investigated, especially its significant positive correlation with the summer rainfall in the Yangtze River Basin the following year (Huang et al. 2006; Wu and Qian 2003). Combined effects of long-term and short-term variability on EPEs can be studied further. Besides the atmospheric conditions investigated in this paper, other atmospheric conditions representing short-term variability, including dewpoint temperature (Lepore et al. 2016), convective inhibition (CIN) (Lepore et al. 2016) and K-index (Davies et al. 2013), can also be considered in the analyses of EPEs.

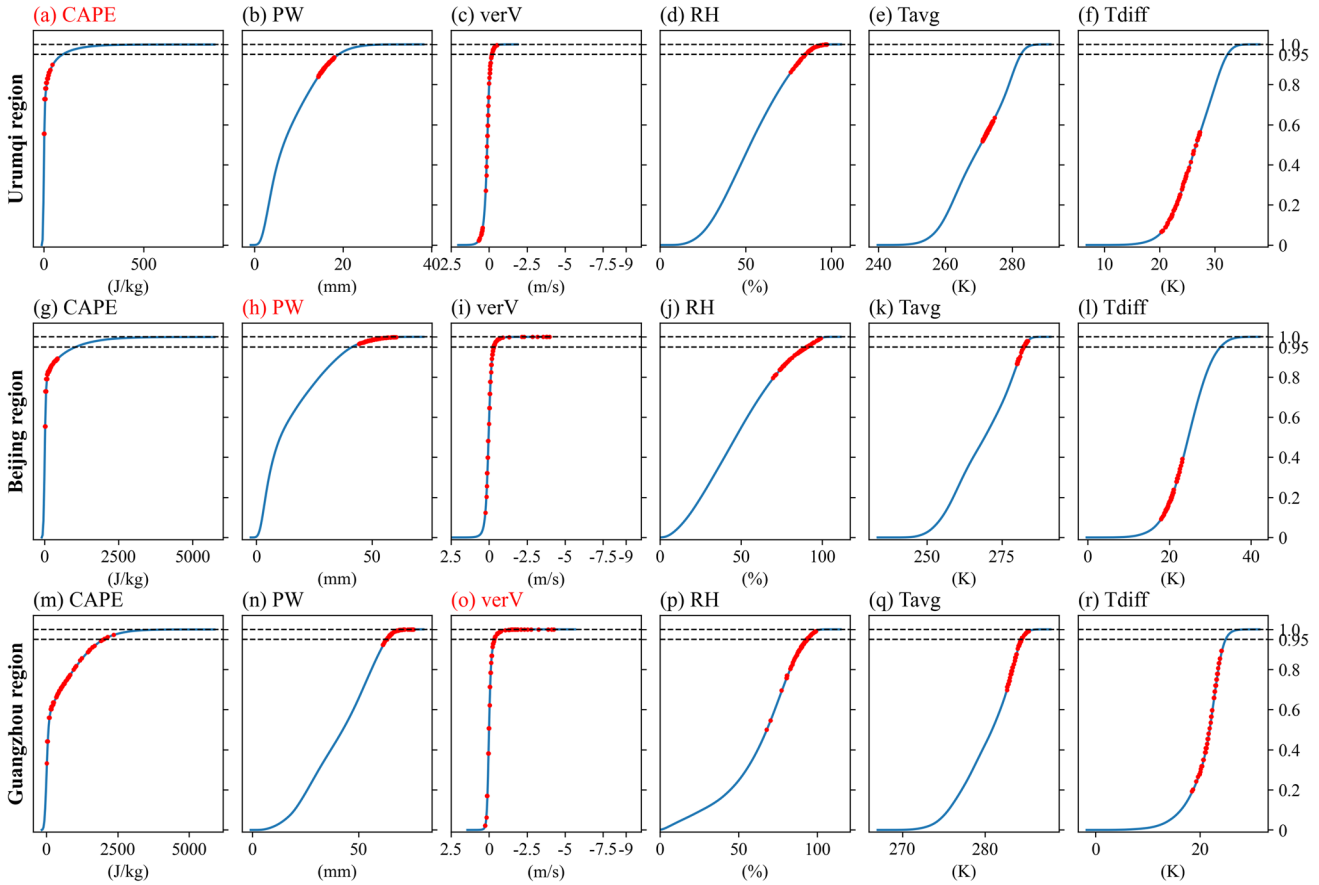

Fig. 9 The CDF curves of **a** CAPE, **b** PW, **c** verV, **d** RH, **e** Tavg and **f** Tdiff for Urumqi region (first row), Beijing region (second row) and Guangzhou region (third row). The red dots reflect the conditions of these factors during the selected event. The 95% CDF which represents the threshold for the extreme condition is depicted as a dashed line. The red font in the title indicates that the factor is the dominant controlling factor of EPEs in this grid cell

6 Conclusions

This paper has presented an in-depth investigation of the relationships between 72-h EPEs and atmospheric conditions (atmospheric instability, moisture availability and wind convergence) as well as driving variables (vertical velocity, relative humidity and air temperature) for each grid cell in China. The investigation is built upon the classic coincidence probability. That is, by comparing the coincidence probability values obtained from the top events, the annual and seasonal dominant controlling factors of EPEs are identified. The results show that at the annual timescale, Southeast and Southwest China are dominantly controlled by verV, North and Central China by PW and Northwest China by CAPE roughly. From the perspective of driving variables, the findings indicate that verV drives extreme precipitation in most parts of the country, while Tavg takes over as the primary factor in the Qinghai-Tibet Plateau. According to the significance tests, the approach to determining the dominant controlling factor of EPEs is shown to be effective. At the seasonal timescale, the spatial distributions of coincidence probability values and dominant controlling factors exhibit similar patterns as observed throughout the entire year except for DJF. Additionally, the diagnostic plots generated for three case study regions in China provide valuable insights into the temporal evolution of precipitation events, CDF curves of influential factors and dominant controlling factors of EPEs. The diagnostic plots can serve as a practical guide and aid in formulating appropriate strategies to address the challenges posed by EPEs. At the same time, the analysis framework that is based on the estimation of classic coincidence probability can also be applied to storms at various durations. Overall, this paper contributes to validate the dominant controlling factor of EPEs for the whole of China as well as identify their spatial patterns, which can be important for rainstorm forecasting and disaster risk reduction.

Supplementary Information The online version contains supplementary material available at https://doi.org/10.1007/s00382-024-07143-z.

Acknowledgements This research is supported by the National Key Research and Development Program of China (2021YFC3001000), the National Natural Science Foundation of China (51979295, 51861125203 and U1911204) and the Guangdong Provincial Department of Science and Technology (2019ZT08G090).

Author contributions QO and TZ conceptualized the design of the study. SW, YL, YW, BL and XC participated in statistical analyses. QO and TZ performed the storyline simulations, analysis, visualization, and wrote the first draft. All authors contributed to the main manuscript text and reviewed the manuscript.

Funding Ministry of Science and Technology of the People's Republic of China (2021YFC3001000); National Natural Science Foundation of China (51979295); Guangdong Science and Technology Department (2019ZT08G090).

Data availability The reanalysis data sets in this study are obtained from ECMWF-ERA5 (Hersbach et al. 2020, available at https://cds.climate.copernicus.eu/cdsapp#!/dataset/reanalysis-era5-pressure-levels?tab=overview).

Declarations

Conflict of interest The authors have no competing interests as defined by Springer, or other interests that might be perceived to influence the results and/or discussion reported in this paper.

References

Ali H, Mishra V (2018) Contributions of dynamic and thermodynamic scaling in subdaily precipitation extremes in India. Geophys Res Lett 45(5):2352–2361. https://doi.org/10.1002/2018GL077065

Ali H, Fowler HJ, Lenderink G, Lewis E, Pritchard D (2021) Consistent large-scale response of hourly extreme precipitation to temperature variation over land. Geophys Res Lett. https://doi.org/10.1029/2020GL090317

Betts AK, Chan DZ, Desjardins RL (2019) Near-surface biases in ERA5 over the Canadian prairies. Front Environ Sci. https://doi.org/10.3389/fenvs.2019.00129

Brooks HE, Lee JW, Craven JP (2003) The spatial distribution of severe thunderstorm and tornado environments from global reanalysis data. Atmos Res 67–68:73–94. https://doi.org/10.1016/S0169-8095(03)00045-0

Charba JP (1977) Operational system for predicting thunderstorms two to six hours in advance

Chen H (2013) Projected change in extreme rainfall events in China by the end of the 21st century using CMIP5 models. Chin Sci Bull 58(12):1462–1472. https://doi.org/10.1007/s11434-012-5612-2

Chen X, Hossain F (2018) Understanding model-based probable maximum precipitation estimation as a function of location and season from atmospheric reanalysis. J Hydrometeorol 19(2):459–475. https://doi.org/10.1175/JHM-D-17-0170.1

Chen X, Hossain F (2019) Understanding future safety of dams in a Changing climate, vol 100. American Meteorological Society, Boston, pp 1395–1404

Cipolla G, Francipane A, Noto LV (2020) Classification of extreme rainfall for a Mediterranean region by means of atmospheric circulation patterns and reanalysis data. Water Resour Manage 34(10):3219–3235. https://doi.org/10.1007/s11269-020-02609-1

Davies L, Jakob C, May P, Kumar VV, Xie S (2013) Relationships between the large-scale atmosphere and the small-scale convective state for Darwin, Australia. J Geophys Res Atmos 118(20):11,511–534, 545. https://doi.org/10.1002/jgrd.50645

Dong W, Lin Y, Wright JS, Xie Y, Yin X, Guo J (2019) Precipitable water and CAPE dependence of rainfall intensities in China. Clim Dyn 52(5–6):3357–3368. https://doi.org/10.1007/s00382-018-4327-8

Donges JF, Donner RV, Trauth MH, Marwan N, Schellnhuber H, Kurths J (2011) Nonlinear detection of paleoclimate-variability transitions possibly related to human evolution. Proc Natl Acad Sci 108(51):20422–20427. https://doi.org/10.1073/pnas.1117052108

Dube RK, Rao GSP (2005) extreme weather events over India in the last 100 years. https://api.semanticscholar.org/CorpusID:131542400

Formayer H, Fritz A (2017) Temperature dependency of hourly precipitation intensities – surface versus cloud layer temperature. Int J Climatol 37:1

Gaál L, Molnar P, Szolgay J (2014) Selection of intense rainfall events based on intensity thresholds and lightning data in Switzerland. Hydrol Earth Syst Sci 18(5):1561–1573. https://doi.org/10.5194/hess-18-1561-2014

Gao X, Guo M, Yang Z, Zhu Q, Xu Z, Gao K (2020) Temperature dependence of extreme precipitation over mainland China. J Hydrol 583:124595. https://doi.org/10.1016/j.jhydrol.2020.124595

Gorman PAO (2012) Sensitivity of tropical precipitation extremes to climate change. Nat Geosci 5(10):697–700. https://doi.org/10.1038/ngeo1568

Hardwick Jones R, Westra S, Sharma A (2010) Observed relationships between extreme sub-daily precipitation, surface temperature, and relative humidity. Geophys Res Lett. https://doi.org/10.1029/2010GL045081

Hersbach H, Bell B, Berrisford P, Hirahara S, Horányi A, Muñoz Sabater J, Nicolas J, Peubey C, Radu R, Schepers D, Simmons A, Soci C, Abdalla S, Abellan X, Balsamo G, Bechtold P, Biavati G, Bidlot J, Bonavita M, Chiara G, Dahlgren P, Dee D, Diamantakis M, Dragani R, Flemming J, Forbes R, Fuentes M, Geer A, Haimberger L, Healy S, Hogan RJ, Hólm E, Janisková M, Keeley S, Laloyaux P, Lopez P, Lupu C, Radnoti G, Rosnay P, Rozum I, Vamborg F, Villaume S, Thépaut JN (2020) The ERA5 global reanalysis. Q J R Meteorol Soc 146(730):1999–2049. https://doi.org/10.1002/qj.3803

Hersbach H, Bell B, Berrisford P, Balsamo G, Horányi A, Muñoz Sabater J, Nicolas J, Peubey C, Radu R, Rozum I, Schepers D, Simmons A, Soci C, Dee D, Thépaut JN (2023a) ERA5 hourly data on single levels from 1940 to present. Copernicus Climate Change Service (C3S) Climate Data Store (CDS)

Hersbach H, Bell B, Berrisford P, Balsamo G, Horányi A, Muñoz Sabater J, Nicolas J, Peubey C, Radu R, Rozum I, Schepers D, Simmons A, Soci C, Dee D, Thépaut JN (2023b) ERA5 hourly data on pressure levels from 1940 to present. Copernicus Climate Change Service (C3S) Climate Data Store (CDS)

Hoeppe P (2016) Trends in weather related disasters—consequences for insurers and society. Weather Clim Extrem 11:70–79. https://doi.org/10.1016/j.wace.2015.10.002

Huang R, Chen J, Zhou L, Zhang Q (2003) Studies on the relationship between the severe climatic disasters in China and the East Asia Climate System. Chin J Atmos Sci 27(4):770–787

Huang R, Cai R, Chen J, Zhou L (2006) Interdecaldal variations of drought and flooding disasters in china and their association with the East Asian climate system. Chin J Atmos Sci 30(5):730–743

Huang Z, Zhao T, Xu W, Cai H, Wang J, Zhang Y, Liu Z, Tian Y, Yan D, Chen X (2022) A seven-parameter Bernoulli-Gamma-Gaussian model to calibrate subseasonal to seasonal precipitation forecasts. J Hydrol 610:127896. https://doi.org/10.1016/j.jhydrol.2022.127896

Lang Y, Jiang Z, Wu X (2022) Investigating the linkage between extreme rainstorms and concurrent synoptic features: a case study in Henan, Central China. Water 14(7):1065. https://doi.org/10.3390/w14071065

Lepore C, Veneziano D, Molini A (2015) Temperature and CAPE dependence of rainfall extremes in the eastern United States. Geophys Res Lett 42(1):74–83. https://doi.org/10.1002/2014GL062247

Lepore C, Allen JT, Tippett MK (2016) Relationships between hourly rainfall intensity and atmospheric variables over the contiguous United States. J Clim 29(9):3181–3197. https://doi.org/10.1175/JCLI-D-15-0331.1

Li Y, Deng Y, Yang S, Zhang H, Ming Y, Shen Z (2019) Multi-scale temporal-spatial variability of the East Asian summer monsoon frontal system: observation versus its representation in the GFDL HiRAM. Clim Dyn 52(11):6787–6798. https://doi.org/10.1007/s00382-018-4546-z

Li C, Zhao T, Shi C, Liu Z (2021) Assessment of precipitation from the CRA40 dataset and new generation reanalysis datasets in the global domain. Int J Climatol 41(11):5243–5263. https://doi.org/10.1002/joc.7127

Li H, Moisseev D, Luo Y, Liu L, Ruan Z, Cui L, Bao X (2023) Assessing specific differential phase (KDP)-based quantitative precipitation estimation for the record- breaking rainfall over Zhengzhou city on 20 July 2021. Hydrol Earth Syst Sci 27(5):1033–1046. https://doi.org/10.5194/hess-27-1033-2023

Liu J, Pei Y, Mei C, Liu C (2023) Waterlogging cause and disaster prevention and control of "7·20" torrential rain in Zhengzhou. J Zhengzhou Univ (engineering Science) 44(02):38–45

Loikith PC, Lintner BR, Sweeney A (2017) Characterizing large-scale meteorological patterns and associated temperature and precipitation extremes over the Northwestern United States using self-organizing maps. J Clim 30(8):2829–2847. https://doi.org/10.1175/JCLI-D-16-0670.1

Loriaux JM, Lenderink G, Siebesma AP (2016) Peak precipitation intensity in relation to atmospheric conditions and large-scale forcing at midlatitudes. J Geophys Res Atmos 121(10):5471–5487. https://doi.org/10.1002/2015JD024274

Mahapatra B, Walia M, Saggurti N (2018) Extreme weather events induced deaths in India 2001–2014: trends and differentials by region, sex and age group. Weather Clim Extrem 21:110–116. https://doi.org/10.1016/j.wace.2018.08.001

McErlich C, McDonald A, Schuddeboom A, Vishwanathan G, Renwick J, Rana S (2023) Positive correlation between wet-day frequency and intensity linked to universal precipitation drivers. Nat Geosci 16(5):410–415. https://doi.org/10.1038/s41561-023-01177-4

Min S, Zhang X, Zwiers FW, Hegerl GC (2011) Human contribution to more-intense precipitation extremes. Nature 470(7334):378–381. https://doi.org/10.1038/nature09763

Mishra V, Wallace JM, Lettenmaier DP (2012) Relationship between hourly extreme precipitation and local air temperature in the United States. Geophys Res Lett. https://doi.org/10.1029/2012GL052790

Molnar P, Fatichi S, Gaál L, Szolgay J, Burlando P (2015) Storm type effects on super Clausius-Clapeyron scaling of intense rainstorm properties with air temperature. Hydrol Earth Syst Sci 19(4):1753–1766. https://doi.org/10.5194/hess-19-1753-2015

Muller CJ, Gorman PAO, Back LE (2011) Intensification of precipitation extremes with warming in a cloud-resolving model. J Clim 24(11):2784–2800. https://doi.org/10.1175/2011JCLI3876.1

Prein AF, Rasmussen RM, Ikeda K, Liu C, Clark MP, Holland GJ (2017) The future intensification of hourly precipitation extremes. Nat Clim Chang 7(1):48–52. https://doi.org/10.1038/nclimate3168

Rammig A, Wiedermann M, Donges JF, Babst F, von Bloh W, Frank D, Thonicke K, Mahecha MD (2015) Coincidences of climate extremes and anomalous vegetation responses: comparing tree ring patterns to simulated productivity. Biogeosciences 12(2):373–385. https://doi.org/10.5194/bg-12-373-2015

Rudolph JV, Friedrich K (2014) Dynamic and thermodynamic predictors of vertical structure in radar-observed regional precipitation. J Clim 27(5):2143–2158. https://doi.org/10.1175/JCLI-D-13-00239.1

Shen C, Zha J, Wu J, Zhao D, Azorin-Molina C, Fan W, Yu Y (2022) Does CRA-40 outperform other reanalysis products in evaluating near-surface wind speed changes over China? Atmos Res 266:105948. https://doi.org/10.1016/j.atmosres.2021.105948

Tao S, Wei J (2007) Correlation between Monsoon surge and heavy rainfall causing flash-flood in Southern China in Summer. Meteorol Mon 33(3):10–18

Thompson HD, Déry SJ, Jackson PL, Laval BE (2020) A synoptic climatology of potential seiche-inducing winds in a large intermontane lake: Quesnel Lake, British Columbia, Canada. Int J Climatol 40(14):5973–5986. https://doi.org/10.1002/joc.6560

Urraca R, Huld T, Gracia-Amillo A, Martinez-de-Pison FJ, Kaspar F, Sanz-Garcia A (2018) Evaluation of global horizontal irradiance estimates from ERA5 and COSMO-REA6 reanalyses using ground and satellite-based data. Sol Energy 164:339–354. https://doi.org/10.1016/j.solener.2018.02.059

Vanden Broucke S, Wouters H, Demuzere M, van Lipzig NPM (2019) The influence of convection-permitting regional climate modeling on future projections of extreme precipitation: dependency on topography and timescale. Clim Dyn 52(9):5303–5324. https://doi.org/10.1007/s00382-018-4454-2

Visser JB, Kim S, Wasko C, Nathan R, Sharma A (2022) The impact of climate change on operational probable maximum precipitation estimates. Water Resour Res. https://doi.org/10.1029/2022WR032247

Wei P, Xu X, Xue M, Zhang C, Wang Y, Zhao K, Zhou A, Zhang S, Zhu K (2023) On the key dynamical processes supporting the 21.7 Zhengzhou record-breaking hourly rainfall in China. Adv Atmos Sci 40(3):337–349. https://doi.org/10.1007/s00376-022-2061-y

Wu T, Qian Z (2003) The relation between the Tibetan Winter Snow and the Asian Summer Monsoon and rainfall: an observational investigation. J Clim 16(12):2038–2051. https://doi.org/10.1175/1520-0442(2003)016%3c2038:TRBTTW%3e2.0.CO;2

Wu J, Gao X, Giorgi F, Chen D (2017) Changes of effective temperature and cold/hot days in late decades over China based on a high resolution gridded observation dataset. Int J Climatol 37:788–800. https://doi.org/10.1002/joc.5038

Xiong S, Zhao T, Guo C, Tian Y, Yang F, Chen W, Chen X (2023) Evaluation and attribution of trends in compound dry-hot events for major river basins in China. Sci China Earth Sci. https://doi.org/10.1007/s11430-022-1174-7

Yang E, Kim HM, Kim D (2022) Development of East Asia regional reanalysis based on advanced hybrid gain data assimilation method and evaluation with E3DVAR, ERA-5, and ERA-Interim reanalysis. Earth Syst Sci Data 14(4):2109–2127. https://doi.org/10.5194/essd-14-2109-2022

Zhan D, Ye S (2000) Engineering hydrology. China Water Power Press, Beijing

Zheng J, Yin Y, Li B (2010) A new scheme for climate regionalization in China. Acta Geogr Sin 65(1):3–12

Zhong S, Qian Y, Zhao C, Leung R, Yang X (2015) A case study of urbanization impact on summer precipitation in the Greater Beijing Metropolitan Area: urban heat island versus aerosol effects. J Geophys Res Atmos 120(20):903–910. https://doi.org/10.1002/2015JD023753

Zhou Y, Peng T, Shi R (2019) Research progress on risk assessment of heavy rainfall and flood disasters in China. Torrent Rain Disast 38(5):494–501. https://doi.org/10.3969/j.issn.1004-9045.2019.05.011

Zhu Y, Wang H, Zhou W, Ma J (2011) Recent changes in the summer precipitation pattern in East China and the background circulation. Clim Dyn 36:1463–1473. https://doi.org/10.1007/s00382-010-0852-9

Zhu X, Lee S, Wen X, Ji Z, Lin L, Wei Z, Zheng Z, Xu D, Dong W (2021) Extreme climate changes over three major river basins in China as seen in CMIP5 and CMIP6. Clim Dyn 57(3):1187–1205. https://doi.org/10.1007/s00382-021-05767-z